A new bohaiornithid-like bird from the Lower Cretaceous of China fills a gap in enantiornithine disparity

Authors: Wang, Xuri, Cau, Andrea, Luo, Xiaoling, Kundrát, Martin, Wu, Wensheng, et al.

Source: Journal of Paleontology, 96(4) : 961-976

Published By: The Paleontological Society

URL: https://doi.org/10.1017/jpa.2022.12

Journal of Paleontology, 96(4), 2022, p. 961–976

0022-3360/22/1937-2337
doi: 10.1017/jpa.2022.12

JOURNAL OF PALEONTOLOGY
A PUBLICATION OF THE Paleontological SOCIETY

A new bohaiornithid-like bird from the Lower Cretaceous of China fills a gap in enantiornithine disparity

Xuri Wang,[1,2] Andrea Cau,[3] Xiaoling Luo,[4] Martin Kundrát,[5] Wensheng Wu,[2] Shubin Ju,[1,6] Zhen Guo,[2] Yichuan Liu,[1,6] and Qiang Ji[2]*

[1]Key Laboratory of Stratigraphy and Paleontology of the Ministry of Natural Resources, Institute of Geology, Chinese Academy of Geological Sciences, 26 Baiwanzhuang Road, Beijing 100037, China <147966459@qq.com>
[2]Hebei GEO University, 136 Huai An Road, Shijiazhuang 050031, Hebei Province, China <1417555452@qq.com> <guozhen@hgu.edu.cn> <jiqiang@hgu.edu.cn>
[3]Independent, Imbriani M.R. Street, Parma 43125, Italy <cauand@gmail.com>
[4]Research Center of Development, China Geological Survey, Courtyard 45 Fuwai Street, Beijing 100037, China <1256053083@qq.com>
[5]Center for Interdisciplinary Biosciences, Technology and Innovation Park, University of Pavol Jozef Šafárik, 04154, Košice, Slovakia <martin.kundrat@upjs.sk>
[6]China University of Geosciences, 29 Xueyuan Road, Beijing 100083, China <251603098@qq.com> <1976570361@qq.com>

Abstract.—A new enantiornithine, *Musivavis amabilis* n. gen. n. sp., is reported from the Lower Cretaceous Jehol Biota in western Liaoning, China. The new taxon is similar to the bohaiornithids in the robust subconical teeth, bluntly expanded omal ends of the furcula, caudolaterally oriented lateral trabeculae with triangular distal ends of the sternum, and a robust second pedal digit. Yet it differs from members of Bohaiornithidae in several features recalling other enantiornithine lineages, such as the acuminate rostral ramus of maxilla, the shape of the coracoid lateral margin, the presence of craniolateral processes on the sternum, the proportions of the manual phalanges, and the unspecialized third pedal ungual phalanx. A comprehensive phylogenetic analysis of Mesozoic birds shows that homoplasy significantly affects the reconstruction of enantiornithine relationships. When all phylogenetic characters are considered of equal weight, *Musivavis* is reconstructed in a lineage related to a radiation of large-bodied enantiornithines including Bohaiornithidae and Pengornithidae. Alternative scenarios based on progressive downweighting of the homoplastic characters support more basal placements of the pengornithids among Enantiornithes, but do not alter the affinity of *Musivavis* as a member of the "bohaiornithid-grade" group.

UUID: http://zoobank.org/617c7062-21ab-4d33-ae80-4edf5a129683

Introduction

Enantiornithes is the most speciose clade of Cretaceous birds, with >50 genera named to date (Zhou, 2014; O'Connor et al., 2016; Chiappe et al., 2019; Wang and Zhou, 2019; Xu et al., 2020). Fossils belonging to this group have been reported from every continent except Antarctica (Chiappe and Meng, 2016). The Early Cretaceous Jehol Biota in northeastern China has produced more than half of the known enantiornithine birds (Hu et al., 2015, 2020; Wang and O'Connor, 2017; Wang and Zhou, 2019). Most specimens from the Jehol Biota are nearly complete and often preserve plumage or other soft tissue remains. The abundant fossil birds from the Jehol Biota not only have increased the taxonomic diversity of the Cretaceous birds, but also have provided critical information regarding aspects of the ontogeny, sexual dimorphism, reproduction, and ecology (Zhang and Zhou, 2000; Zhou and Zhang, 2006; O'Connor et al., 2009; Zheng et al., 2011, 2014; Wang and Zhou, 2019; Bailleul et al., 2020). With increasing information provided by continuous discoveries of enantiornithines, the analysis and interpretation of their evolutionary history, interrelationships, and ecology have been proved challenging tasks (Wang and O'Connor, 2017; Chiappe et al., 2019; O'Connor et al., 2020). The majority of the Jehol Biota enantiornithines have been referred to four main groups: the small-bodied and relatively unspecialized cathayornithids (sensu Wang and Liu, 2016; see also O'Connor and Dyke, 2010), the long-snouted longipterygids (O'Connor et al., 2009), and two groups of large-bodied taxa—the bohaiornithids (M. Wang et al., 2014) and the pengornithids (X.-L. Wang et al., 2014). The monophyly of some of these groups is debated, in particular for the cathayornithids and the bohaiornithids, because both might represent evolutionary grades among Euenantiornithes (see Wang and Liu, 2016; Chiappe et al., 2019).

*Corresponding author.

Here, we describe a new enantiornithine bird from the Lower Cretaceous Jiufotang Formation in western Liaoning of China. The new enantiornithine combines size and peculiar features previously seen in small-bodied enantiornithines and in the cathayornithids with features usually identified as diagnostic of the bohaiornithid lineage.

Material and methods

The new specimen (MHGU-3000) described here was collected from the Lower Cretaceous Jiufotang Formation (Aptian) at Shangheshou locality, Chaoyang City of western Liaoning, China (41°36′N, 120°23′E) (Fig. 1). In order to determine the ontogenetic age of MHGU-3000, we took a sample from the middle shaft of the left tibiotarsus of the type specimen. The sample was embedded in one-component resin (EXAKT Technovit 7200) and hardened in a light polymerization device (EXAKT 520). The histological section was cut transversely using an accurate circular saw (EXAKT 300CP). The section was ground using the EXAKT 400CS grinding system until the desired optical contrast was obtained. The histological section was examined by light microscopy under both normal and polarized light (ZEISS AX10). Images of each slice were captured using a digital camera (ZEISS AxioCam MRc5) and further processed using Adobe Photoshop and CorelDRAW X5 software. Histological measurements were taken from digitized cross sections using ImageJ.

In order to place MHGU-3000 in a phylogenetic context, we coded it as an Operational Taxonomic Unit (OTU), and included into a data set expanded from the phylogenetic analysis of X.-R. Wang et al. (2020; modified from Cau, 2018) focusing on Mesozoic short-tailed birds. The matrix consists of 86 OTUs scored for 1837 binary character statements (Supplementary data 1, 2). The long-tailed bird *Archaeopteryx* was used as outgroup to root the tree. All analyses performed 1000 'New Technology search' replications using the TNT software (Goloboff et al., 2008) in order to explore tree islands, and then explored more exhaustively running a Tree-Bisection-Reconnection analysis using the sampled trees as starting point. We explored the effect of homoplastic characters on pygostylian relationships performing four analyses using the "Extended Implied Weighting" function in TNT, setting the concavity parameter *K* value (which defines the downweighting of the characters according to their homoplasy) as, alternatively, 5 (most aggressive downweighting setting used), 10, 15, and 20 (less aggressive downweighting setting used). The four replications using the "Extended Implied Weighting" function followed the same search protocol used in the first (unweighted) analysis.

Following O'Connor and Dyke (2010), we consider *Vescornis* a junior synonym of *Hebeiornis*. The clade name Bohaiornithidae refers to the least inclusive clade containing *Bohaiornis* and *Shenqiornis* (M. Wang et al., 2014), whereas the informal terms "bohaiornithid-like" and "bohaiornithid-grade" refer to bohaiornithids and to those enantiornithines sharing a subset of the diagnostic features of Bohaiornithidae regardless to their inclusion in the latter clade (e.g., *Gretcheniao*, Chiappe et al., 2019).

Repositories and institutional abbreviations.—Types and other specimens examined in this study are deposited in the following institutions: The Museum of Hebei GEO University (MHGU), Shijiazhuang City, Hebei Province, China; Beijing Museum of Natural History (BMNH), Beijing, China; or the Institute of Vertebrate Paleontology and Paleoanthropology (IVPP), Beijing, China.

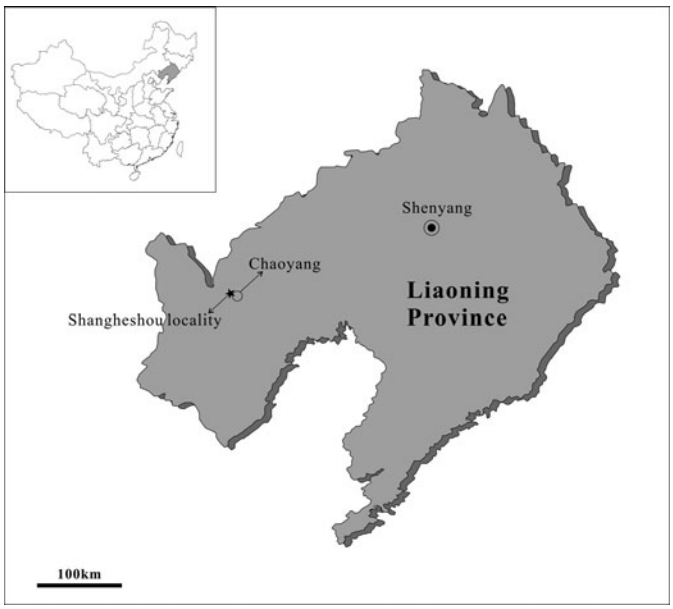

Figure 1. Map of Liaoning Province, China, showing the Shangheshou locality in Chaoyang City where the holotype (MHGU-3000) of *Musivavis amabilis* n. gen. n. sp. was recovered.

Systematic paleontology

Avialae Gauthier, 1986
Pygostylia Chiappe, 2002
Ornithothoraces Chiappe, 1995
Enantiornithes Walker, 1981
Genus *Musivavis* new genus

Type species.—*Musivavis amabilis* n. gen. n. sp., only known species, from the Aptian of northeastern China.

Diagnosis.—As for the type species, by monotypy.

Etymology.—The generic name is derived from the Latin "*musivum*" (mosaic, decoration with small stone *tesserae*) and "*avis*" (bird).

Remarks.—As for the type species.

Musivavis amabilis new species
Figures 2–12; Table 1

Holotype and only known specimen.—MHGU-3000, a nearly complete and articulated skeleton preserved in a single slab.

Diagnosis.—*Musivavis amabilis* n. gen. n. sp. can be referred to Enantiornithes by possessing several synapomorphies of this

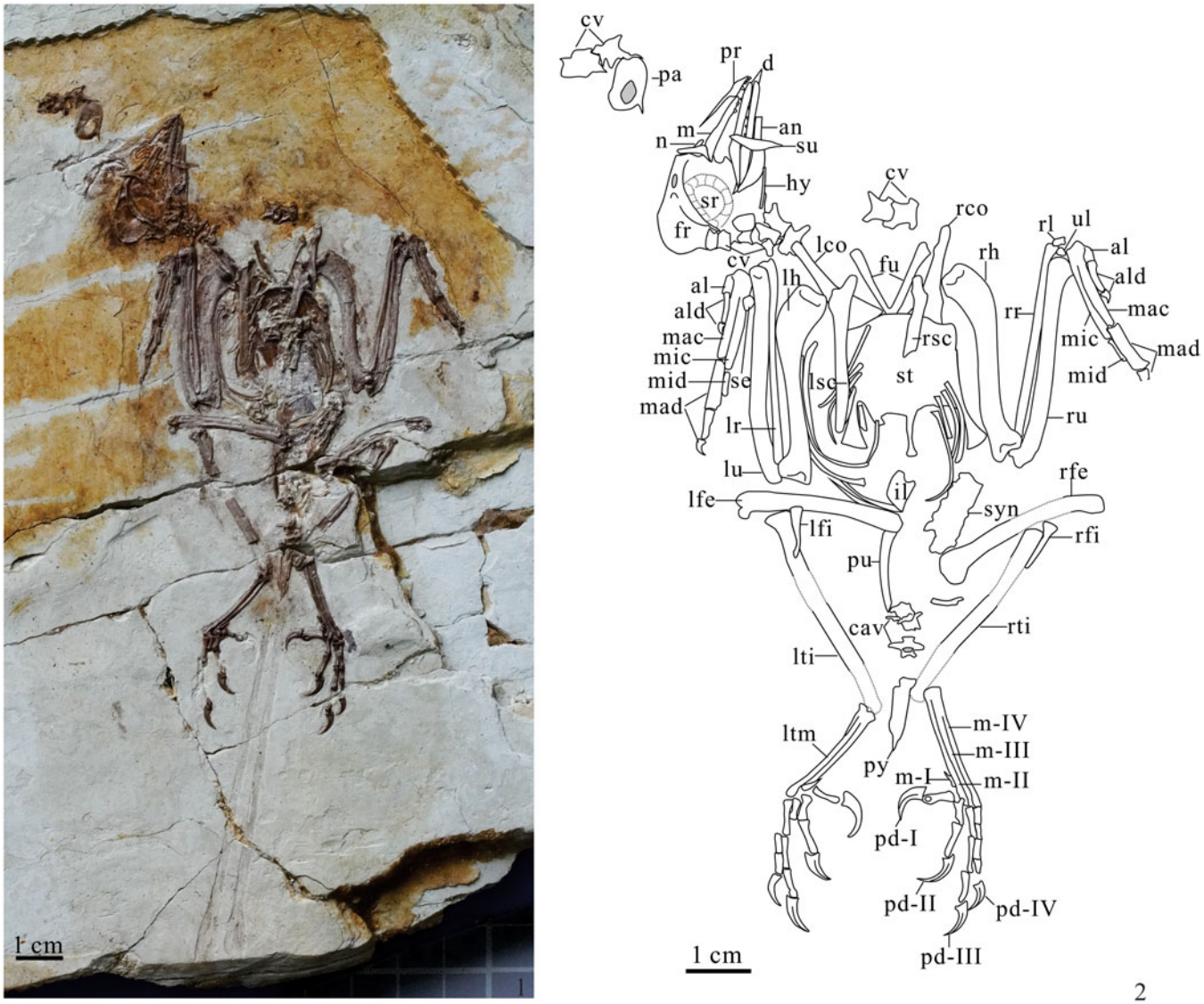

Figure 2. Holotype (MHGU-3000) of *Musivavis amabilis* n. gen. n. sp. from the Early Cretaceous Jiufotang Formation (Aptian). (**1**) photograph; (**2**) line drawing. Abbreviations: al, alular metacarpal; ald, alular digits; an, angular; cav, caudal vertebrae; cv, cervical vertebrae; d, dentary; fu, furcula; fr, frontal; hy, hyoid; il, ilium; lco, left coracoid; lfe, left femur; lfi, left fibula; lh, left humerus; lr, left radius; lsc, left scapula; lti, left tibiotarsus; ltm, left tarsometatarsus; lu, left ulna; m, maxilla; m- Ⅰ–Ⅳ, metatarsal Ⅰ-Ⅳ; mac, major metacarpal; mad, major manual digits; mic, minor metacarpal; mid, minor manual digits; n, nasal; pa, parietal; pd- Ⅰ–Ⅳ, pedal digit Ⅰ-Ⅳ; pr, premaxilla; pu, pubis; py, pygostyle; rco, right coracoid; rfe, right femur; rfi, right fibula; rh, right humerus; rl, radiale; rr, right radius; rsc, right scapula; rti, right tibiotarsus; ru, right ulna; se, semilunate carpal; sr, scleral ring; st, sternum; su, surangular; syn, synsacrum; ul, ulnare.

clade, such as the sternum with nearly equal length and width, the "Y"-shaped furcula with a long hypocleideum, the minor metacarpal extending farther distally than the major metacarpal, and the fourth metatarsal relatively thin (Chiappe and Walker, 2002). It can be further referred to the "Bohaiornithidae-grade" group by possessing some of the diagnostic features of this family, such as the subconical teeth with tapered and slightly caudally recurved tips, the sternum with lateral trabecula projected caudolaterally, the omal end of furcular ramus with blunt expansion, and the tapered pygostyle without abrupt distal constriction (M. Wang et al., 2014). It is distinguishable from the bohaiornithids by possessing the following unique combination of features (local autapomorphies denoted by asterisks): the pygostyle abruptly tapers distally (shared with *Gretcheniao*); the sulcus excavating the epicleideal ramus of the furcula is very deep and extends distally onto the proximal third of the hypocleideum*; a sharp keel runs along the whole ventral surface of the furcula, from the junction of the epicleideal rami to the distal tip of the hypocleideum; the flat cranial margin of the sternum becomes curved near the craniolateral process*; the sternum possesses craniolaterally projected craniolateral processes* (in bohaiornithids, only *Zhouornis* possesses craniolateral processes, which project laterally); the xiphoid process of the sternum extends nearly to the same level of the distal end of the lateral trabecula and expands as a blunt distal end (shared with *Bohaiornis*); and the first alular phalanx bears a transversally expanded proximal end followed by a gracile shaft, resulting in a concave proximomedial corner of the bone*.

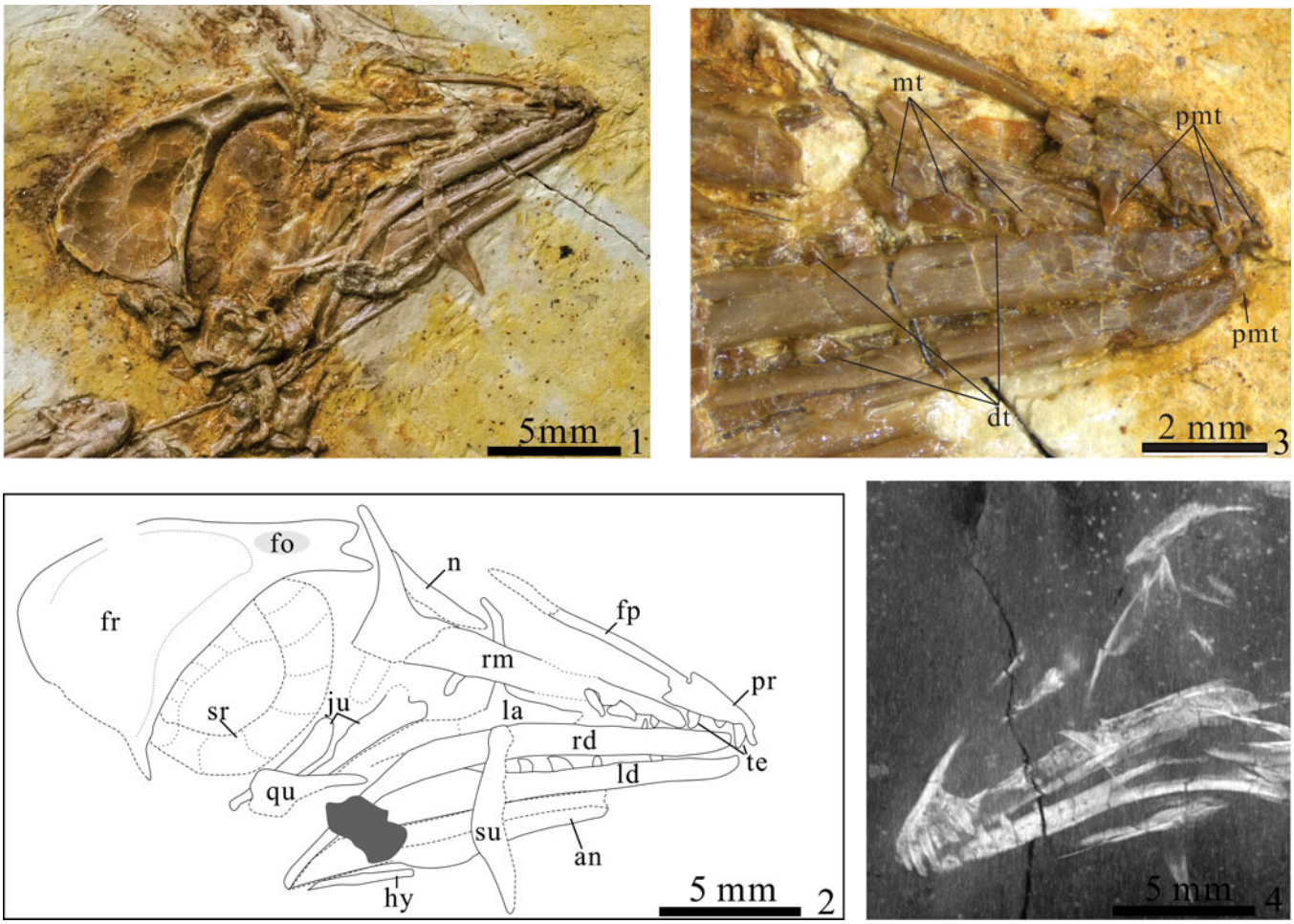

Figure 3. Skull of the holotype (MHGU-3000) of *Musivavis amabilis* n. gen. n. sp. in ventrolateral view. (**1**) photograph; (**2**) line drawing; (**3**) close-up of the rostral portion; (**4**) micro-CT scan of the rostral portion. Abbreviations: an, angular; dt, dentary teeth; fo, frontal fossa; fp, frontal process; fr, frontal; hy, hyoid; ju, jugal; la, lacrimal; ld, left dentary; mt, maxillary teeth; n, nasal; pmt, premaxillary teeth; pr, premaxilla; qu, quadrate; rd, right dentary; rm, right maxilla; sr, scleral ring; su, surangular; te, teeth.

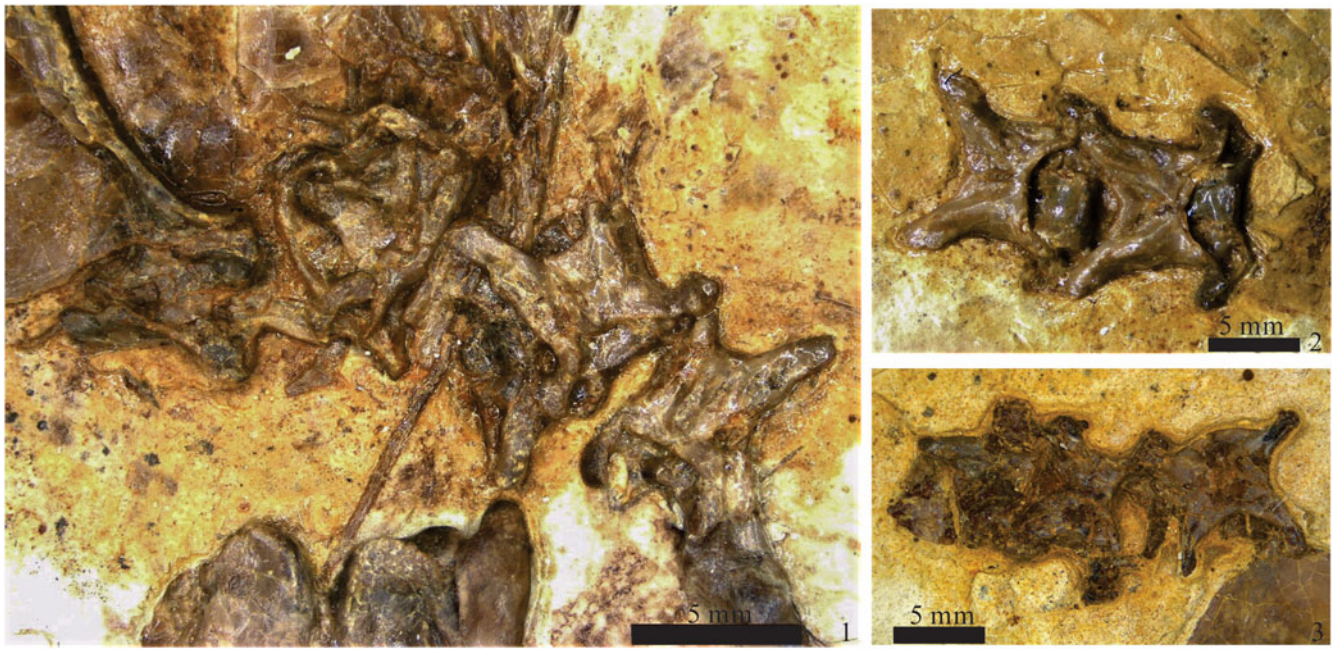

Figure 4. Cervical vertebrae of the holotype (MHGU-3000) of *Musivavis amabilis* n. gen. n. sp.

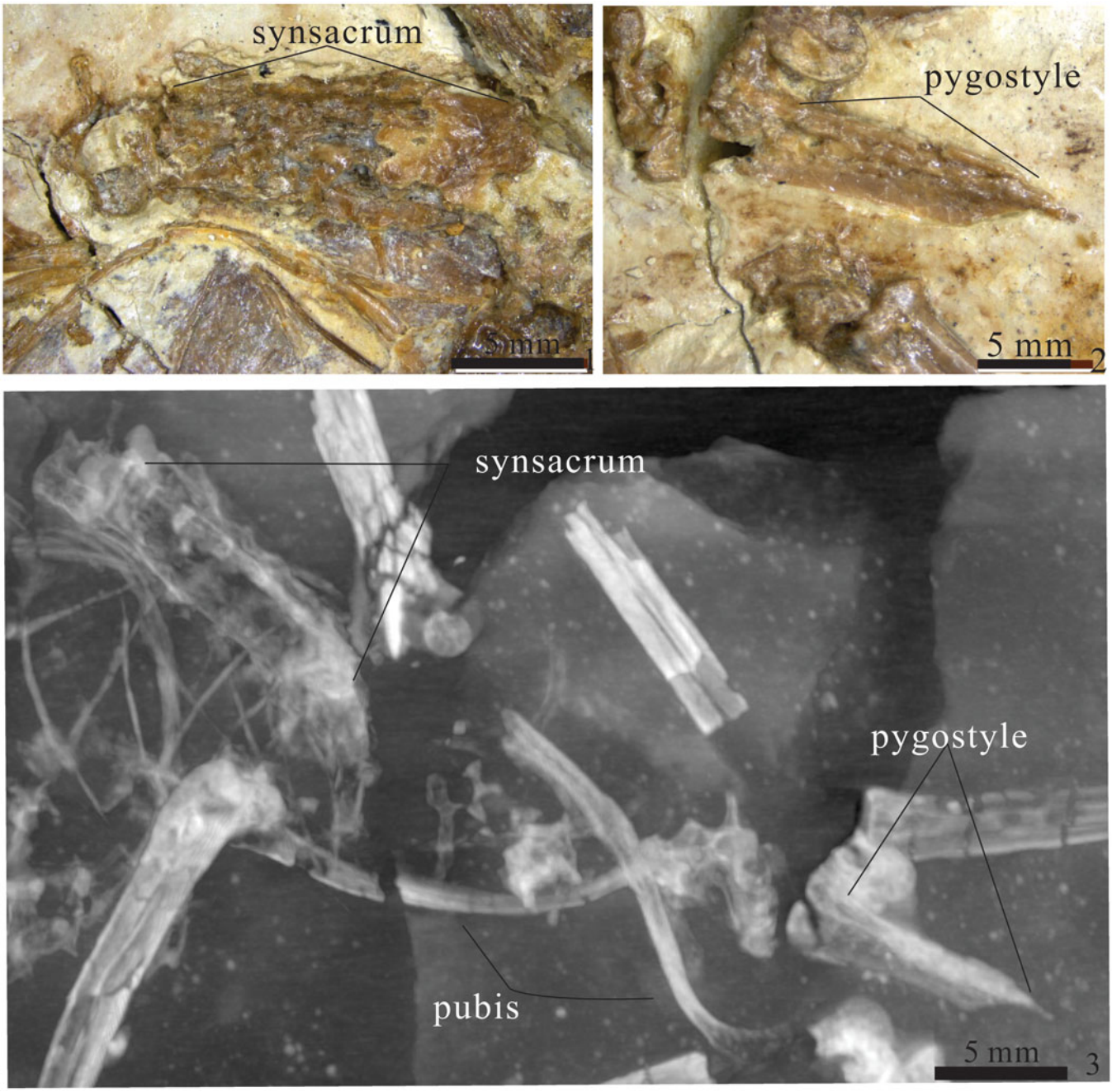

Figure 5. Synsacrum, pygostyle, and pubis of the holotype (MHGU-3000) of *Musivavis amabilis* n. gen. n. sp. (**1**) photograph of synsacrum; (**2**) photograph of pygostyle; (**3**) CT scan.

Occurrence.—The holotype was recovered from the Lower Cretaceous Jiufotang Formation (Aptian) at Shangheshou locality, Chaoyang City, Liaoning Province, China.

Description.—The skull is mainly preserved in ventrolateral view (Fig. 3). The right premaxilla is preserved in lateral view. It gradually tapers rostrally and slightly expands dorsoventrally in the middle part, differing from the robust premaxilla of the bohaiornithids (M. Wang et al., 2014) and the elongated premaxilla of the longipterygids (O'Connor and Chiappe, 2011), but similar in overall proportions to those of the Cathayornithidae (Wang and Liu, 2016). The frontal process of the right premaxilla is elongate and projects caudodorsally, but does not extend to the orbit, comparable with the condition in bohaiornithids (M. Wang et al., 2014; Hu et al., 2020). As in other bohaiornithid-like taxa, the maxilla is robust, with a straight ventral margin and gently expanded dorsal margin. The nasal is too broken to determine the exact anatomical features. The right lacrimal is preserved in dorsolateral view and appears to be "T"-shaped. The rostral ramus is oriented rostroventrally, but the exact length cannot be determined because it is overlapped by the right maxilla. The caudal ramus projects caudodorsally and the ventral ramus extends caudoventrally. The dorsal margin is concave at

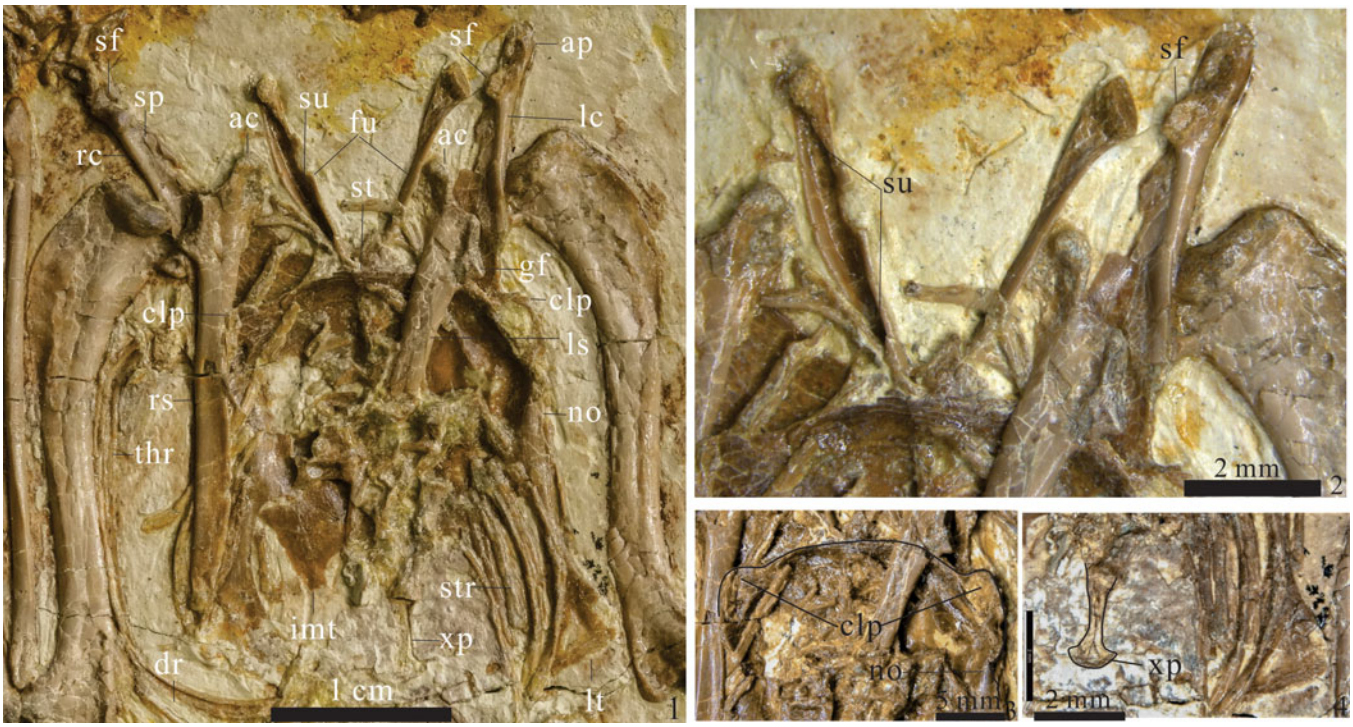

Figure 6. Pectoral girdle and sternum of the holotype of *Musivavis amabilis* n. gen. n. sp. (MHGU-3000). (**1**) photograph; (**2**) close-up of the furcula and coracoid; (**3**) close-up of the cranial margin of the sternum; (**4**) close-up of the xiphoid process of the sternum. Abbreviations: ac, acromial process of the scapula; ap, acrocoracoid process of the coracoid; clp, craniolateral process of the sternum; dr, dorsal ribs; fu, furcula; gf, glenoid facet of the scapula; imt, intermediate trabecula; lc, left coracoid; ls, left scapula; lt, lateral trabecula of the sternum; no, notch of the sternum; rc, right coracoid; rs, right scapula; sf, scapular facet; sp, supracoracoidal nerve foramen; st, sternum; str, sternal ribs; su, sulci of the furcular rami; thr, thoracic ribs; xp, xiphoid process of the sternum.

the middle part, as reported in *Pengornis*, *Longusunguis*, and *Parabohaiornis*, but different from the straight margin of *Pterygornis* (M. Wang et al., 2016). The frontal is rostrocaudally elongate, narrow rostrally, and domed caudally, as in other enantiornithines (e.g., *Protopteryx*, *Parapengornis*, *Bohaiornis*, and *Shangyang*; Zhang and Zhou, 2000; M. Wang et al., 2014; Hu et al., 2015; Wang and Zhou, 2019). The rostral portion of the frontal is rectangular-shaped, with a triangular depression, a feature that is also present in the enantiornithine *Piscivorenantiornis inusitatus* (Wang and Zhou, 2020) and the ornithuromorph *Archaeorhynchus spathula* (Zhou et al., 2013). A deep oval fossa is located between the forked rostral end and the expanded dome of the frontal. This fossa, which is natural judging by the smooth margins and surface, has not been documented previously in Mesozoic birds. However, it is premature to conclude this oval fossa is a diagnostic character because the skulls of fossil birds are typically incompletely preserved or exposed in views that prevented observing this region. It probably represents the depression of the olfactory bulb and the articulation with the mesethmoid (Baumel et al., 1993). The ventral margin of the frontal is slightly concave and forms the dorsal margin of the orbit. The dorsal margin of the frontal is robust and strongly expanded dorsally. The sclerotic ring is nearly completely preserved and, as preserved, is composed of 14 thin imbricated elements. The ventral seven sclerotic ossicles are much larger than the dorsal seven ossicles. The square-shaped sclerotic ossicles are plate-like and have rounded margins, similar to those of *Longusunguis* (Hu et al., 2020). The quadrate is partly exposed in lateral view. No orbital process can be observed due to the overlapping by other bones. The rostral portions of the two strap-like jugals are exposed in lateral view, and disarticulated from the jugal processes of the maxillae. The right parietal is displaced above the skull and close to three cervical vertebrae. This condition proves that the parietal is not fused with the frontal. The palatal elements are mostly overlapped by the cervical vertebrae.

Figure 7. CT renderings of the coracoid and furcula of the holotype (MHGU-3000) of *Musivavis amabilis* n. gen. n. sp. (**1**) Left coracoid in dorsomedial view; (**2**) left coracoid in ventromedial view; (**3**) right coracoid in lateromedial view; (**4**) right coracoid in ventromedial view; (**5**) furcula in dorsal view; (**6**) furcula in ventral view.

The two dentaries are not fused at the symphysial area. The rostral end of the dentary tapers rostrodorsally. In its rostral two-thirds, the ventral margin of the dentary is straight, while the caudal one-third is slightly curved and tapered caudoventrally, as in other enantiornithines (Chiappe et al., 2019). A series of nutrient foramina is visible on the rostral part of the lateral surface of the right dentary. The right angular is robust, with tapered rostral end and expanded caudal end, measuring

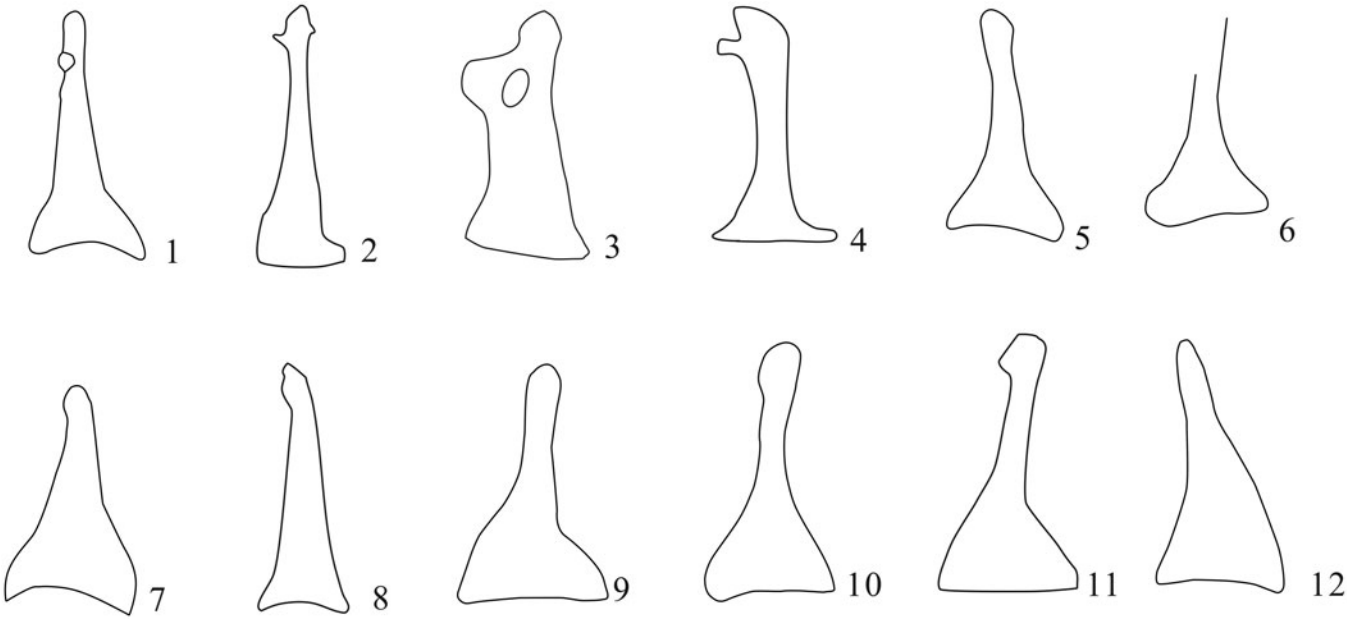

Figure 8. Comparative line drawings of coracoid of the holotype of *Musivavis amabilis* n. gen. n. sp. (MHGU-3000) and selected Mesozoic birds. (**1**) *Musivavis amabilis* n. gen. n. sp.; (**2**) *Protopteryx fengningensis* Zhang and Zhou, 2000; (**3**) *Kompsornis longicaudus* X.-R. Wang et al., 2020; (**4**) *Abitusavis lii* M. Wang et al., 2020; (**5**) *Bohaiornis guoi* Hu et al., 2011; (**6**) *Parabohaiornis martini* M. Wang et al., 2014; (**7**) *Longusunguis kurochkini* M. Wang et al., 2014; (**8**) *Gretcheniao sinensis* Chiappe et al., 2019; (**9**) *Sulcavis geeorum* O'Connor et al., 2013; (**10**) *Shenqiornis mengi* X.-R. Wang et al., 2010; (**11**) *Eoenantiornis buhleri* Hou et al., 1999; (**12**) *Eocathayornis walkeri* Zhou, 2002.

~75% the length of the right dentary. The right surangular is preserved in lateral view and is shorter than the right angular, with extremely tapered rostral and caudal ends, and dorsally expanded middle part. The left surangular is articulated with the left dentary. The hyoids are straight and slender.

Teeth are present in the premaxilla, maxilla, and dentary (Fig. 3). As in most enantiornithines, the premaxillae possess four teeth, which are small (< 1 mm) and subconical in shape. The tooth root is rectangular-like in lateral view and nearly the same height as the crown. There is a slight constriction between

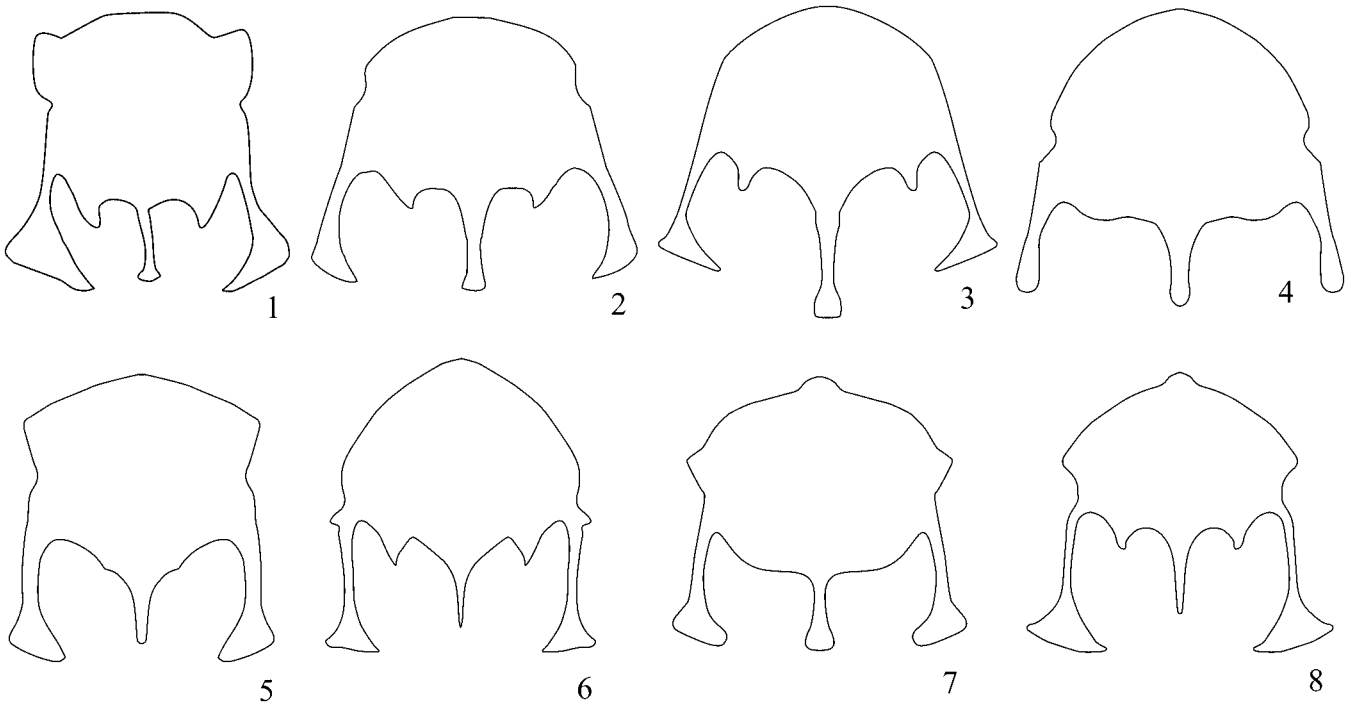

Figure 9. Comparative line drawings of sternum of the holotype (MHGU-3000) of *Musivavis amabilis* n. gen. n. sp. and selected enantiornithines. (**1**) *Musivavis amabilis* n. gen. n. sp.; (**2**) *Bohaiornis guoi*; (**3**) *Parabohaiornis martini*; (**4**) *Longusunguis kurochkini*; (**5**) *Zhouornis hani* Zhang et al., 2013; (**6**) *Cathayornis yandica* Zhou et al., 1992; (**7**) *Eocathayornis walkeri*; (**8**) *Houornis caudatus* Wang and Liu, 2016.

Figure 10. Left forelimb of the holotype (MHGU-3000) of *Musivavis amabilis* n. gen. n. sp. in ventral view. (**1**) Photograph; (**2**) close-up of the proximal ends of the left metacarpals; (**3**) close-up of the proximal ends of the right metacarpals. Abbreviations: al, alular metacarpal; ald-1–2, alular digit 1–2; bi, bicipital crest; hu, humerus; ma, major metacarpal; mad-1–3, major manual digit 1–3; mi, minor metacarpal; mid-1, minor manual digit 1; ra, radius; ul, ulna; se, semilunate carpal.

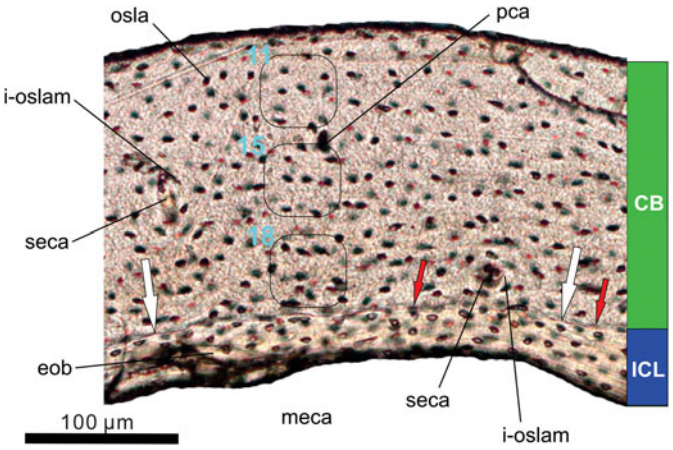

Figure 12. Histology of the left tibiotarsus of the holotype (MHGU-3000) of *Musivavis amabilis* n. gen. n. sp. Transverse section of the midshaft level is viewed in transmitted light. Note decreasing counts of osteocyte lacunae per area, for example from 18 in the innermost cortex to 11 in the outermost cortex (outlined areas in CB). The white arrows point an irregular interface between the cortical and endosteal bones, whereas the red arrows mark partially eroded osteocyte lacunae. Abbreviations: CB, cortical bone; eob, endosteal bone; ICL, inner circumferential layer; i-oslam, ill-developed osteonal lamellae; meca, medullary cavity; osla, osteocyte lacuna; pca, primary osteonal (neurovasular) canal; seca, secondary osteonal canal.

the root and crown. The crown slightly expands basally and becomes sharp apically with the caudally recurved labial side and the relatively straight lingual side. The premaxillary teeth are most similar in size and morphology to the teeth of *Eoenantiornis* (Zhou et al., 2005). They strongly differ from the large robust teeth in bohaiornithids, the large recurved and laterally compressed teeth of *Longipteryx*, and the numerous small and blunt teeth of *Pengornis* (O'Connor et al., 2013). The interalveolar space is nearly equal to the crown width. Six teeth are visible in the right maxilla. The completely exposed maxillary teeth are much larger than the premaxillary teeth. The dentary teeth are smaller than the premaxillary and maxillary teeth but similar in morphology.

The cervical vertebrae are partially disarticulated (Fig. 4). The anterior four cervical vertebrae are preserved between the skull and the right coracoid. Three cervical vertebrae are preserved above the skull, and two additional cervical vertebrae are preserved near the furcula and the left coracoid. The cervical vertebrae are short and robust, with prominent ventral keels and zygapophyses. Three thoracic vertebrae are visible. These exhibit rectangular centra and distinctly concave posterior intercentral facets, as in most enantiornithines (Chiappe and Walker, 2002). The synsacrum is completely fused and includes at least seven vertebrae, with no more-detailed features that can be observed due to poor preservation (Fig. 5). The free caudal vertebrae are poorly preserved. The pygostyle is preserved in latero-ventral view and abruptly tapers distally (Fig. 5), similar to the shape of the distal end in *Gretcheniao* (Chiappe et al., 2019), and in contrast to the gently tapered distal end in other bohaiornithids (M. Wang et al., 2014), and different from the more conspicuous constrictions in most enantiornithine pygostyles (e.g., *Boluochia*, *Shanweiniao*, and *Rapaxavis*; Zhou, 1995; O'Connor et al., 2009, 2011). The exact length of the pygostyle cannot be determined due to the broken proximal end. Two thoracic ribs are preserved next to the left humerus, which extend dorsally, defining an obtuse angle with the corresponding straight shaft (Fig. 6), differing from the acute angle in *Parabohaiornis* (M. Wang et al., 2014). Six sternal ribs are

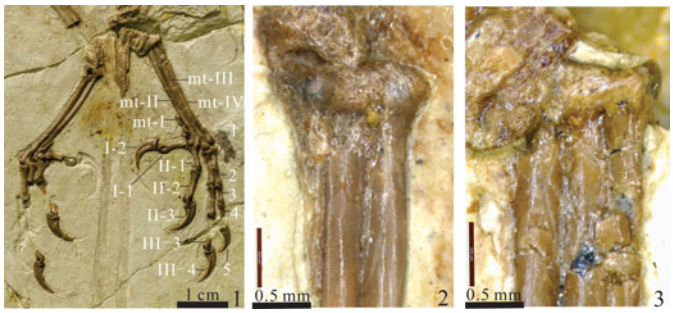

Figure 11. Feet of the holotype (MHGU-3000) of *Musivavis amabilis* n. gen. n. sp. (**1**) Photograph; (**2**) close-up of the proximal end of the left tarsometatarsus; (**3**) close-up of the proximal end of the right tarsometatarsus. Abbreviations: mt-I–IV, metatarsal I–IV; I-1–2, pedal digit I-1-2; II-1–2–3, pedal digit II-1–2–3; III-3–4, pedal digit III-3–4; 1–2–3–4–5, pedal digit IV-1–2–3–4–5.

Table 1. Measurements (in mm) of the holotype (MHGU-3000) of *Musivavis amabilis* n. gen. n. sp. Abbreviations: L, left; R, right; # indicates preserved length.

Element	Length	Element	Length
skull	30	tibia	33
sternum	15	fibula	8#(R)
furcular ramus	12	metatarsal Ⅰ	4(R)
coracoid	14(R)	pedal digit Ⅰ-1	5(R)
scapular	26(L)	pedal digit Ⅰ-2	7(R)
humerus	30	metatarsal Ⅱ	19(R)
ulna	33	pedal digit Ⅱ-1	4(R)
radius	33	pedal digit Ⅱ-2	6(R)
metacarpal Ⅰ	4	pedal digit Ⅱ-3	6(R)
manual digit Ⅰ-1	5(L)	metatarsal Ⅲ	19(R)
manual digit Ⅰ-2	2(L)	pedal digit Ⅲ-1	6(R)
metacarpal Ⅱ	14(L)	pedal digit Ⅲ-2	5(R)
manual digit Ⅱ-1	8(L)	pedal digit Ⅲ-3	5(R)
manual digit Ⅱ-2	5(L)	pedal digit Ⅲ-4	5(R)
manual digit Ⅱ-3	2(L)	metatarsal Ⅳ	18(R)
metacarpal Ⅲ	16(L)	pedal digit Ⅳ-1	3(R)
manual digit Ⅲ-1	4(L)	pedal digit Ⅳ-2	3(R)
pygostyle	12#	pedal digitⅣ-3	3(R)
synsacrum	15	pedal digit Ⅳ-4	4(R)
femur	27	pedal digit Ⅳ-5	4(R)

preserved adjacent to the right side of the sternum. The middle three sternal ribs are longer and more recurved than the cranial and caudal sternal ribs. Six sternal ribs are also preserved close to the left side of the sternum, but are partially overlapped by the left scapula or are broken.

Both coracoids are preserved in dorsomedial view and are strut-like (Figs. 6, 7). The supracoracoid nerve foramen is visible in the right coracoid. The foramen is placed inside a distinct fossa excavating the medial margin of the coracoid. The acrocoracoid process is well developed and rectangular, with the long axis aligned with the long axis of the coracoid shaft. The coracoid bears a prominent tubercle forming the convex scapular facet, a feature present in the majority of enantiornithines (Chiappe and Walker, 2002; M. Wang et al., 2014). The scapular facet prominently projects medially. CT scans reveal the sternal margin of the coracoid, which is relatively concave and slightly expanded mediolaterally (Fig. 7; Supplementary data 3, 4): the ratio of sternal margin width to coracoid shaft length is 44%. This condition is similar to most bohaiornithids but different from that of *Gretcheniao*, in which the sternal margin is less expanded mediolaterally (Fig. 8) (M. Wang et al., 2014; Chiappe et al., 2019; Hu et al., 2020). The scapula is straight and long, nearly 87% the length of the humerus. The acromial process is well developed and aligned to the long axis of the scapular shaft. The glenoid fossa is prominently concave and oriented laterally. The scapular morphology is similar to those of most bohaiornithids, *Eoenantiornis*, and *Pterygornis* (M. Wang et al., 2016), but different from the sagittally curved scapula of *Zhouornis*, *Fortunguavis*, and *Dunhuangia* (M. Wang et al., 2015), and from the laterally projected acromial process of *Gretcheniao* (Chiappe et al., 2019). A shallow elliptical fossa excavates longitudinally the distal half of the lateral surface of the scapula. CT scan reveals that the furcula is Y-shaped with a prominent hypocleideum, nearly 70% the length of the furcular ramus (Fig. 7; Supplementary data 5, 6). The hypocleideum is comparable in extent to other enantiornithines, being shorter than the furcular ramus, and gradually tapered distally. The epicleideal rami are relatively straight, with expanded and robust omal ends, forming an angle of ~45° at the junction, a value which is the same as that of *Gretcheniao* and *Zhouornis*, and smaller than that of *Shenqiornis* (50°), *Sulcavis* (60°), *Bohaiornis* (60°), and *Parabohaiornis* (60°). The expanded omal ends of the furcular rami are also consistent with those in Bohaiornithidae, but different from the tapered omal ends of *Gretcheniao* and most enantiornithines (Chiappe et al., 2019). The right furcular ramus, which is exposed in visceral view, shows a deep fusiform sulcus running along the whole ramus and extending onto the proximal third of the hypocleideum (Fig. 7; Supplementary data 5, 6). In other enantiornithines, the sulcus is either shallower or less expanded distally, not reaching the hypocleidum (e.g., *Parapengornis*; Hu et al., 2015). The sulci on both furcular rami are clearly visible in the CT scans (Fig. 7; Supplementary data 5, 6). A sharp keel runs along the ventral surface of the furcula, from the junction of the epicleideal rami to the distal tip of the hypocleideum (Supplementary data 5, 6).

The sternal plate, exposed in dorsal (visceral) view, is short and broad, with the width and length subequal (Fig. 6), as in other members of Enantiornithes (Chiappe and Walker, 2002). The cranial margin is flat at midline and curved near the craniolateral process. In other bohaiornithid-like taxa, craniolateral processes are present in *Zhouornis* (Zhang et al., 2013), but absent in *Bohaiornis*, *Parabohaiornis*, and *Longusunguis* (M. Wang et al., 2014). Furthermore, the process extends craniolaterally and describes a nearly right angle, different from the laterally projected craniolateral process of *Zhouornis*, but similar to that of *Pterygornis* and *Shangyang* (M. Wang et al., 2016; Wang and Zhou, 2019). Craniolateral processes are hypothesized to ossify from separate centers and develop late in certain taxa (e.g., *Rapaxavis* and *Concornis*; M. Wang et al., 2015), which suggests that *Musivavis* n. gen. was not juvenile at the time of death. There is a very small notch on the lateral margin, similar to the condition in *Longusunguis* and *Zhouornis*, but different from the smooth lateral margin in *Bohaiornis* and *Parabohaiornis* (Hu et al., 2020). The lateral trabecula is oriented caudolaterally and expands into a triangular process distally that expands more medially (resulting in a more acuminate medial corner) than laterally, a morphology consistent with most bohaiornithids (except for *Longusunguis*) and several Cathayornithidae (e.g., *Cathayornis*, *Eocathayornis*, and *Houornis*) (M. Wang et al., 2015). As in *Bohaiornis*, *Eocathayornis*, *Shanweiniao*, and *Longirostravis*, the xiphoid process extends nearly to the same level as the distal end of lateral trabecula and slightly expands transversely to be a blunt distal end (Zhang et al., 2013). The xiphoid process projects farther caudally than the lateral trabecula and flares slightly mediolaterally at the distal end in *Parabohaiornis* (M. Wang et al., 2014). In other enantiornithines, the xiphoid process is tapered distally (e.g., *Cathayornis*, *Houornis*, *Eoenantiornis*, *Longipteryx*, and *Rapaxavis*; Zhang et al., 2013; M. Wang et al., 2015). As in *Bohaiornis*, *Pterygornis*, *Cathayornis*, and *Eoenantiornis*, the intermediate trabecula is short and oriented mediocaudally, contrary to the laterocaudally oriented intermediate trabecula in *Parabohaiornis* (M. Wang et al., 2014) (Fig. 9).

The left forelimb is nearly complete and articulated (Fig. 10). It is nearly the same length as the hindlimb ([humerus + ulna + carpometacarpus]/[femur + tibiotarsus + metatarsal III] = 1.0). The intermembral index is similar to those of *Gretcheniao* (1.1) and Bohaiornithidae (0.9–1.1) (Chiappe et al., 2019; Hu et al., 2020), a smaller value than that of other enantiornithine groups (e.g., >1.3 in Pengornithidae and ~1.2 in Longipterygidae) (X.-R. Wang et al., 2015; Hu et al., 2020).

The humerus is slightly S-shaped and shorter than the ulna and radius. Proximally, the deltopectoral crest expands dorsally and decreases caudally at the first one-third of the humeral shaft. A prominent excavation runs along the dorsal margin of the deltopectoral crest. The bicipital crest is robust and projects anteroventrally, forming a deep notch with the humeral shaft (Fig. 10). The bicipital crest is not excavated by any fossa or foramen; in contrast, a large and deep fossa excavates the bicipital crest in *Gretcheniao* and *Linyiornis* (Chiappe et al., 2019; Y. Wang et al., 2016). Distally, the dorsal condyle is broad and projects almost perpendicular to the long axis of the humeral shaft. The ventral condyle is not as developed as the dorsal condyle, only slightly extended beyond the distal end of the humerus. A deep and wide notch separates the dorsal and ventral condyles. The ulna is almost the same length as the radius, but

considerably more robust and wider than the latter. The proximal part of the ulna is slightly curved, while the distal part is straight. The radius is relatively gracile and straight. The distal end of the radius seems slightly expanded. The carpals are not fused with the metacarpals. The semilunate carpal is preserved between the ulna and the minor metacarpal. The ulnare overlaps the radiale, preventing a detailed description of size and morphology of the latter.

As in other bohaiornithid-like taxa, the alular metacarpal is sub-rectangular in shape and ~29% the length of the major metacarpal (M. Wang et al., 2014; Chiappe et al., 2019). The proximal ends of the major and minor metacarpals are completely fused together (Fig. 10). The major metacarpal, the most robust element in the metacarpus, is straight and uniformly wide. The minor metacarpal is nearly straight and extends farther distally than the major metacarpal, as in all enantiornithines (Chiappe and Walker, 2002). The relatively straight minor metacarpal and the narrow intermetacarpal space are similar to the condition in *Longipteryx*, *Gretcheniao*, and Bohaiornithidae, but different from other enantiornithines, which bear a more curved minor metacarpal forming the lateral margin of a relatively expanded intermetacarpal space (e.g., *Hebeiornis* and *Eoenantiornis*; M. Wang et al., 2014; Chiappe et al., 2019; Hu et al., 2020).

The phalangeal formula of the manus is thus 2-3-1-X-X, consistent with that of Cathayornithidae, *Eoenantiornis*, *Gretctheniao*, and Bohaiornithidae (Zhou et al., 2005; O'Connor and Dyke, 2010; Chiappe et al., 2019; Hu et al., 2020). As in most enantiornithines, but unlike the bohaiornithids, *Protopteryx*, *Longipteryx*, *Eoenantiornis*, and *Monoenantiornis* (Zhou et al., 2005; Hu and O'Connor, 2017; Hu et al., 2020), the alular digit terminates at two-thirds of the major metacarpal shaft. The shaft of the first phalanx of the alular digit is straight and slender. The proximal end of the phalanx expands transversely, resulting in a prominent medial corner, which describes a gentle concavity with the medial margin of the phalanx shaft. The alular ungual phalanx is smaller than the major ungual phalanx and not as curved as the latter. In the bohaiornithids, the alular ungual phalanx is larger than or equal to the major ungual phalanx (M. Wang et al., 2014; Hu et al., 2020). The first phalanx of the major manual digit is straight and as wide as the major metacarpal, which is also the longest phalanx. The second phalanx of the major manual digit is almost the same length of the first phalanx of the alular manual digit, but much wider and more robust than the latter. Only the first phalanx of the minor manual digit is preserved.

The pelvic elements are not well preserved. Only the proximal end of the ilium and the distal end of the ischium are visible, but few anatomical characteristics can be determined. CT scan reveals that the pubis is long, curved at the middle portion, and bears a distal boot expanded caudodorsally (Fig. 5). The femur is straight and 82% the length of the tibiotarsus, which is similar to most enantiornithines, but less than the pengornithids (where it is >90% tibiotarsus length; Hu and O'Connor, 2017). The femoral head is prominent and projects almost perpendicular to the long axis of the femoral shaft. Distally, the lateral and medial condyles are well developed and separated by a deep notch. The tibiotarsus is long and robust, nearly the same in width as the femur. Only the proximal ends of both fibulae are preserved, and it is difficult to determine the exact length and the extent of the distal end.

The distal tarsals are fused to the proximal ends of metatarsals II–IV (Fig. 11). Metatarsal Ⅰ is short (21% the length of metatarsal Ⅲ) and terminates as a rounded articular facet at the proximal facet of the trochlea of metatarsal Ⅱ. Metatarsals Ⅱ–Ⅳ are completely fused proximally. Metatarsal Ⅲ is the longest and metatarsal Ⅱ is slightly shorter than metatarsal Ⅲ and metatarsal Ⅳ. As in most enantiornithines, metatarsal Ⅳ is much thinner than metatarsals Ⅱ–Ⅲ. The pedal phalangeal formula is 2-3-4-5-X. The first pedal digit is reversed compared with other digits. The second pedal digit is the most robust toe, as in other bohaiornithid-grade taxa (M. Wang et al., 2014), while the third is the longest. All phalanges have well-developed proximal flexor processes. All pedal digits possess sharp and moderately recurved ungual phalanges. Each pedal ungual phalanx bears prominent neurovascular sulci and shows a distinct horny claw. The fourth pedal ungual phalanx is smaller than the other three pedal digit ungual phalanges, a condition approaching that in bohaiornithids (M. Wang et al., 2014). The first pedal ungual phalanx is the most robust ungual phalanx and nearly equal in length to the second and third ungual phalanges, a condition which is different from that in other bohaiornithids, where the third ungual phalanx is the longest, recalling the condition in pengornithids (M. Wang et al., 2014; Hu et al., 2015, 2020).

Etymology.—The specific name is derived from the Latin "*amabilis*" (lovely or beautiful), referring to the exquisite preservation of the holotype.

Remarks.—*Musivavis amabilis* n. gen. n. sp. is much smaller in size than currently known bohaiornithids and pengornithids, and differs from the comparably sized cathayornithids (e.g., *Cathayornis*, *Hebeiornis*, *Sinornis*) in the following features: omal tips of furcula transversely expanded; sternum with craniolateral processes and expanded, triangular-shaped distal end of the lateral trabecula (both features absent in *Hebeiornis*); deltopectoral crest less prominent relative to humerus shaft (more developed in *Cathayornis* and *Sinornis*); minor metacarpal not strongly bowed posteriorly, resulting in a slit-like intermetacarpal space (distinctly bowed in *Cathayornis* and *Sinornis*, resulting in a larger intermetacarpal space); ungual phalanx of major digit more curved than the alular ungual phalanx (less curved in *Hebeiornis*); distal end of metatarsal II subequal in width to distal end of metatarsal III (wider in *Hebeiornis* and *Sinornis*); poorly developed flexor tubercles in the pedal ungual phalanges (more prominent in *Hebeiornis* and *Sinornis*).

Osteohistological assessment of the ontogenetic age

Bone tissue of the left tibiotarsus midshaft was sampled to determine the ontogenetic age of the holotype of *Musivavis amabilis* n. gen. n. sp. (MHGU-3000). A transverse section made through the sample exhibits two different kinds of the bone tissue: cortical bone and endosteal bone (Fig. 12).

The cortical bone (CB) is composed of a thicker (172–186 μm) layer of poorly vascularized bone resembling tissue, which has been considered as parallel-fibered bone in previously described enantiornithines (Chinsamy et al., 1995; M. Wang et al., 2017). A few secondary osteonal canals are present and may indicate an initial reconstruction of the primary bone. However, circumferential osteonal lamellae associated with the canals are rather poorly developed. No outer circumferential layer (OCL) has been recognized in the sample of *Musivavis amabilis* n. gen. n. sp., indicating that active bone deposition had not ceased at the time of death (de Ricqlès et al., 1991).

The endosteal bone (EB) forms the compact avascular inner circumferential layer (ICL), enclosing a large hollowed medullary cavity. The endosteal bone is variably thick (minimum: 30 μm; maximum: 47 μm) and accounts for at least a fifth (~21%) of the total cortex. The cortical and endosteal bones are separated by a scalloping line visible on the section (see white arrows in Fig. 12). This line represents the erosional front. Its irregular shape corresponds to variable rates at which the primary bone was resorbed, and provides evidence about the removal of earliest bone formed in the specimen.

No resting marks, either annuli or lines of arrested growth (LAG), are developed in the sample. This may imply continuous growth in *Musivavis* n. gen. between hatching and death. We cannot rule out, however, that features associated with an early growth interruption were already removed by the bone resorption in the specimen. On the other hand, we may certainly reject the interpretation that the resorption line is a LAG, mainly due to partially eroded osteocyte lacunae being distributed along the erosional front (see red arrows in Fig. 12). Moreover, microlaminar texture and organized osteocyte lacunae characterize the EB, and these characters markedly differ from conditions seen in the CB of *Musivavis* n. gen.

Up to now, a wide range of developmental stages of enantiornithine birds have been examined osteohistologically including: (1) an embryo (Enantiornithes indet.: MUCPv-352-353) from the Late Cretaceous of Argentina (Schweitzer et al., 2002) and another embryonic enantiornithine (*Gobipteryx minuta*, Elzanowski, 1974: ZPALMgR Ⅱ/90) from the Late Cretaceous of Mongolia (Chinsamy and Elzanowski, 2001); (2) an early juvenile (Enantiornithes indet.: MPCM-LH-26189, no LAGs) from the Early Cretaceous of Spain (Knoll et al., 2018); (3) a juvenile (Pengornithidae indet.: IVPP V15576, no LAGs) from the Early Cretaceous of China (O'Connor et al., 2018); (4) a subadult (*Cruralispennia multidonta* M. Wang et al., 2017: IVPP V21711, no LAGs) from the Early Cretaceous of China (M. Wang et al., 2017) and another subadult individual (*Patagopteryx deferrariisi* Alvarenga and Bonaparte, 1992: MACN-N-03, one LAG plus one annulus) from the Late Cretaceous of Argentina (Chinsamy et al., 1995); and (5) some adults from the Early Cretaceous of Spain (cf. *Concornis lacustris* Sanz and Buscalioni, 1992: LH 21006, LAGs = 2; Cambra-Moo et al., 2006) and from the Late Cretaceous of Argentina (Enantiornithes indet.: PVL-4273, five LAGs; Chinsamy et al., 1995).

The absence of annulus or LAG and OCL suggests that the holotype individual was likely an early juvenile stage, whereas the presence of the relatively thick ICL, abundance of non-flattened osteocyte lacunae in the outer cortex, and occurrence of the poorly developed secondary osteons suggest a slightly later developmental age. Compared to other enantiornithines, the advanced degree of co-ossification in the elements of the sternum, carpometacarpus, tibiotarsus, and tarsometatarsus is equivalent to developmental "stage 3" of Hu and O'Connor (2017). Therefore, we suggest that the holotype of *Musivavis amabilis* n. gen. n. sp. perished as a subadult near the ontogenetic stage characterized by the first growth deceleration.

Results of the phylogenetic analyses

The phylogenetic analysis setting all characters as equally weighted found 6400 shortest trees of 1920 steps each (Consistency Index excluding uniformative characters = 0.2765; Retention Index = 0.5131) and resolved MHGU-3000 as nested within a lineage that, in turn, is the sister taxon of the node including Bohaiornithidae and Pengornithidae (Fig. 13). The strict consensus of the shortest trees found shows that the relationships among Enantiornithes are well resolved but weakly supported—a result in agreement with previous studies based on independently developed data sets (e.g., M. Wang et al., 2014). In particular, the analysis supports the monophyly of Longipterygidae, Pengornithidae, and Avisauridae. *Musivavis* n. gen. was found as more closely related to *Dunhuangia* (M. Wang et al., 2015) and *Longusunguis* (M. Wang et al., 2014) than to other enantiornithines, in a lineage that also includes *Houornis* (Wang and Liu, 2016) and, tentatively, *Yungavolucris* (the latter acts as a "wildcard" taxon and might instead be an avisaurid; Chiappe and Walker, 2002). Characters supporting this clade are the straight and elongated frontal process of premaxilla, the dentary with subparallel dorsal and ventral margins along its occlusal part, the expanded omal tips of the furcula, and the strongly curved second pedal ungual phalanx. This clade shares with the "Bohaiornithidae + Pengornithidae" clade a relatively stout first phalanx of the second pedal digit and the more proximal position of the trochlea of metatarsal II relative to those of metatarsal III and IV. These features are relatively homoplastic among Pygostylia (mean homoplasy index = 0.74) and did not support this clade when the dataset was re-analyzed using the "Extended Implied Weighting" function (Fig. 14; Supplementary data 7). When K is set as = 5 or = 10 (most aggressive downweighting settings of the homoplastic characters among those tested), the pengornithids are reconstructed among the earliest-diverging enantiornithine lineages, not closely related to the "bohaiornithid-grade" forms. Under the less aggressive K values used, (i.e., 15 and 20), pengornithids form a more derived enantiornithine lineage, relatively closer to the "bohaiornithid-grade" forms. All analyses using the "Extended Implied Weighting" function reconstructed *Musivavis* n. gen. as sister group of *Dunhuangia*, with the two taxa consistently recovered among the "bohaornithid-grade" group, but nested inside Bohaiornithidae (sensu stricto, M. Wang et al., 2014) only when $K = 15$.

Discussion

The completely fused synsacrum, the extensive fusion among the elements in the sternum, carpometacarpus, tibiotarsus and tarsometatarsus, and the smooth external surface of the long

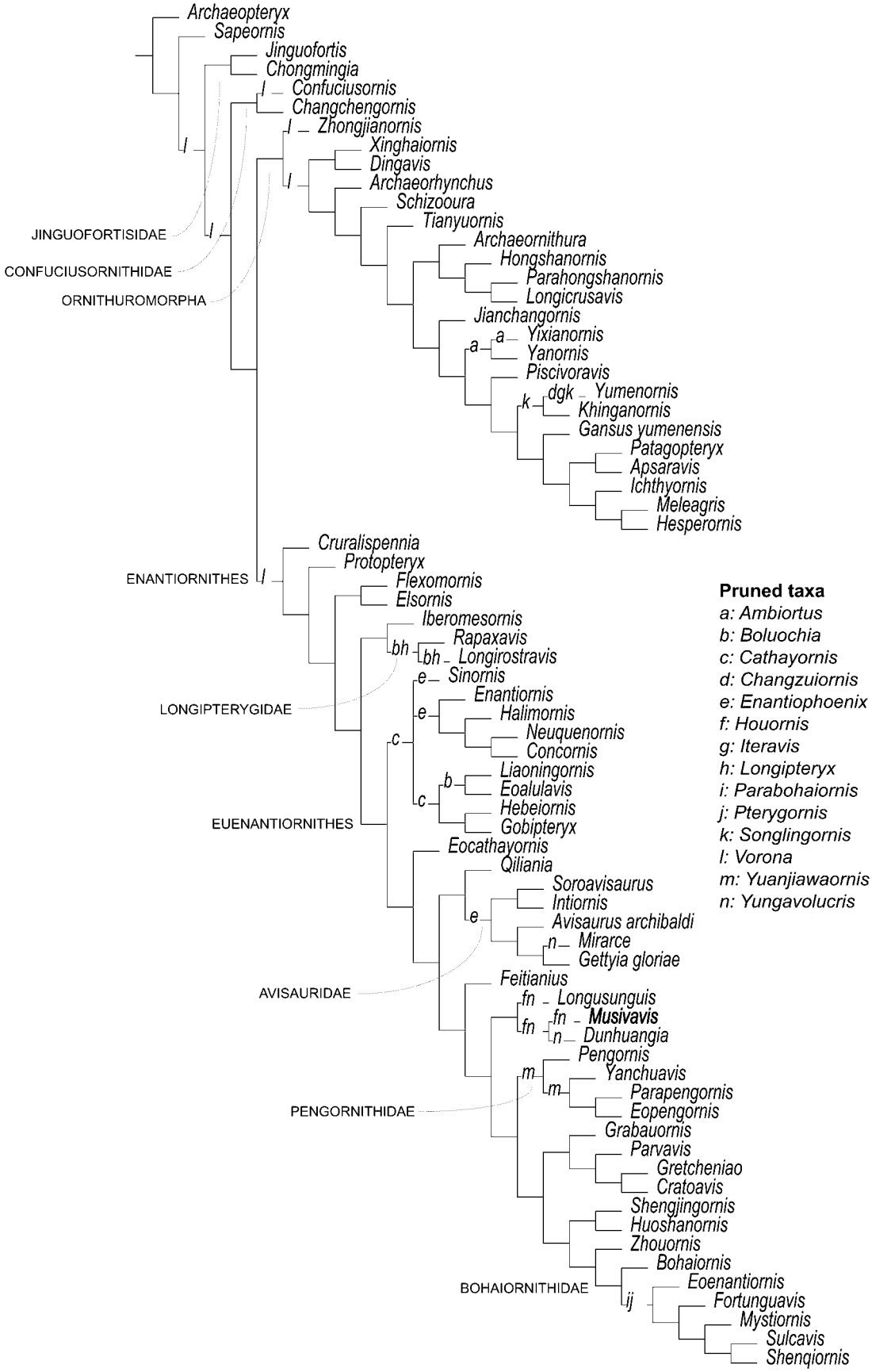

Figure 13. Reduced strict consensus of the shortest trees found by the unweighted analysis after pruning of the "wildcard" taxa. Letters at branches indicate the alternative placements of the "wildcard" taxa.

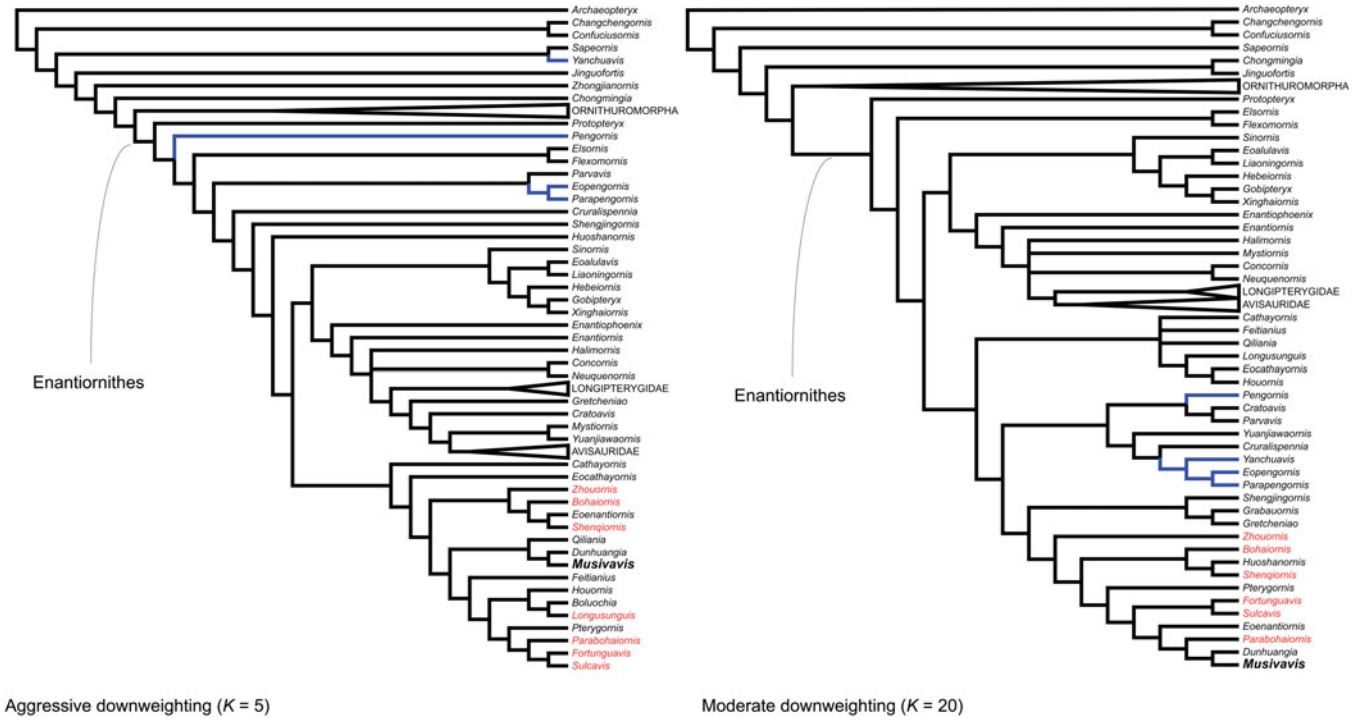

Figure 14. The effect of homoplastic characters in enantiornithine relationships. Two alternative topologies obtained setting an aggressive (left) or moderate (right) downweighting of the characters according to their homoplasy. Note, in particular, the radically different placements of the pengornithids (blue branches) under the two alternative weighting settings. On the contrary, *Musivavis* n. gen. (bold) is consistently found among the least inclusive clade containing the bohaiornithid-like taxa (red). Avisauridae, Longipterygidae, and Ornithuromorpha collapsed for brevity.

bones (i.e, lacking a wrinkled texture) indicate that *Musivavis* n. gen. is more mature skeletally than other recently described juvenile enantiornithines (Wang et al., 2021). The osteohistological analyses also suggest that MHGU-3000 perished during subadult ontogeny. *Musivavis* n. gen. shows typical synapomorphies of Enantiornithes, such as the sternum with nearly equal length and width, the "Y"-shaped furcula with a long hypocleideum, the minor metacarpal extending farther distally than the major metacarpal, and the fourth metatarsal relatively thin (Chiappe and Walker, 2002).

The combination of features in *Musivavis* n. gen. is unique among presently known enantiornithines, supporting the erection of a new taxon. *Musivavis* n. gen. differs from the similar body-sized *Cathayornis* (Zhou et al., 1992), *Houornis* (Hou, 1997; O'Connor and Dyke, 2010; Wang and Liu, 2016), *Hebeiornis* (Xu et al., 1999), *Eoenantiornis* (Zhou et al., 2005), and *Grabauornis* (Dalsätt et al., 2014) in the morphology of the sternum. The deep notch on the lateral margin near the lateral trabecula of the sternum, which is shared by *Cathayornis*, *Houornis*, and *Grabauornis*, is different from the small notch near the craniolateral process in *Musivavis* n. gen. The xiphoid process extends farther distally than the lateral trabecula in *Hebeiornis* and *Eoenantiornis*, while they terminate almost at the same level in *Musivavis* n. gen. In particular, in most enantiornithines the sterna lack distinct craniolaterally projected craniolateral processes (only documented in *Protopteryx*, *Pterygornis*, and *Shangyang*; Wang and Zhou, 2019) and show a uniformly rounded/parabolic cranial margin (e.g., *Protopteryx*, *Longipteryx*, *Cathayornis*, *Bohaiornis*, and *Pterygornis*; M. Wang et al., 2015), differing from the relatively flat cranial

Table 2. Measurements (in mm) of selected skeletal elements of bohaiornithids. *Musivavis* n. gen. was measured directly and the others were cited from M. Wang et al., 2014, and Chiappe et al., 2019.

Element/Taxon	*Shenqiornis* (DNHM D2959)	*Zhouornis* (CNUVB 0903)	*Sulcavis* (BMNH ph805)	*Bohaiornis* (IVPP V17963)	*Longusunguis* (IVPP V17964)	*Parabohaiornis* (IVPP V18691)	*Gretcheniao* (BMMH ph829)	*Musivavis* (MHGU3000)
scapula	39.3	40.7	34.9	36.7	34.7	33.3	~36.8	18.8
coracoid shaft length	26.3	28.4	24.8	25.9	24.2	21.9	29.3	14.0
coracoid medial width	10.7	11.6	12.1	13.1	12.2	12.3	10.5	6.2
medial width/ shaft length of coracoid	0.41	0.41	0.49	0.51	0.50	0.56	0.36	0.44
humerus	46.6	50.6	46.5	52	40.3	43.3	49.7	30
radius	45.8	50.1	47.7	48.5	40.5	40.3	49.2	33
ulna	44.8	53.5	51.1	52.5	43.6	43.8	52.9	33
femur	38.8	44.5	41.3	42.6	35.8	36.0	~42	27
tibiotarsus	?	52.1	47.3	51.3	41.8	40.0	~50	33

margin in *Musivavis* n. gen. The distal expansion of the lateral trabecula and xiphoid process, combined with the size reduction of the alular digit and the more reduced phalangeal formula of the minor digit, further differentiate *Musivavis* n. gen. from *Protopteryx* (Zhang and Zhou, 2000). The same features listed above, and the absence of the peculiar craniomandibular specializations of the longipterygids, preclude the referral of *Musivavis* n. gen. to the latter clade (Zhang et al., 2001). *Musivavis* n. gen. lacks the brachyodont unrecurved teeth and the stouter metatarsus and hallux, which are diagnostic features for *Pengornis* and related taxa (Hu et al., 2015), and clearly differs from the latter in the morphology of the sternum.

Musivavis n. gen. resembles Bohaiornithidae in possessing several diagnostic characteristics of this family, such as the subconical teeth with tapered and slightly caudally recurved tips, the sternum with lateral trabecula strongly projected caudolaterally, and the omal end of the furcular ramus with blunt expansion (M. Wang et al., 2014). Our phylogenetic analyses resolved *Musivavis* n. gen. as consistently nested within the group including the "bohaiornithid-like" taxa (Figs. 13, 14). Furthermore, the "bohaiornithid-like" features of *Gretcheniao*, discussed by Chiappe et al. (2019), result as genuine synapomorphies shared by *Gretcheniao* and the "core bohaiornithids." *Musivavis* n. gen. is much smaller than both *Gretcheniao* (ratio of humerus length = 0.6) and the known bohaiornithids (ratio of humerus length ranges from 0.58–0.8) (Table 2). Bohaiornithidae is diagnosed by, among others, the presence of large subconical teeth (width of the basal part of tooth crown varies from 0.72–0.98 mm), and strongly curved and elongated pedal ungual phalanges (i.e., the third pedal ungual phalanx is at least half the length of the tarsometatarsus) (M. Wang et al., 2014; Hu et al., 2020). The teeth of *Musivavis* n. gen. are small (widest basal part of crown = 0.3 mm), but not as curved as those of other bohaiornithids. The third pedal ungual phalanx of *Musivavis* n. gen. is not significantly elongate, and likely retains the plesiomorphic condition of most enantiornithines. Both the smaller body size and the different tooth and pedal morphologies suggest that *Musivavis* n. gen. was ecologically distinct from the bohaiornithids.

The phylogenetic relationships among the enantiornithines are particularly controversial (e.g., Chiappe and Walker, 2002; O'Connor et al., 2009; O'Connor and Chiappe, 2011; Hu et al., 2015; Chiappe et al., 2019). Our analyses show that homoplasy has a significant effect on the relationships among the main lineages, in particular on the position of Pengornithidae (Hu et al., 2015). The latter group has been reconstructed alternatively as very basal enantiornithines (e.g., X.-L Wang et al., 2014; Chiappe et al., 2019) or as relatively more-derived taxa (O'Connor et al., 2013; M. Wang et al., 2014; Hu et al., 2015). The alternative placements of the pengornithids among Enantiornithes tested in our analyses suggest that the scenarios reconstructing Pengornithidae among late-diverging groups (e.g., relatively close to Bohaiornithidae) are supported by the most-homoplastic characters, in particular those related to scansorial adaptations (i.e., size and proportions of the pedal phalanges). When the phylogenetic weight of those homoplastic characters is mitigated, pengornithids are instead reconstructed as early-diverging enantiornithines—a position that is more in agreement with the retention in these birds of several pygostylian plesiomorphies (e.g., presence of numerous teeth, a high brachial index, the relative elongation of the fibula, the presence of the fifth metatarsal, see X.-L Wang et al., 2014; Hu et al., 2015). In spite of its "mosaic" morphology, the phylogenetic position of *Musivasis* was less affected by alternative assumptions about the weighting of homoplastic characters in the analysis. *Musivavis* n. gen. is consistently reconstructed among the "bohaiornithid-grade" group, although its peculiar morphology challenges it being nested among the "core" Bohaiornithidae (the least inclusive clade containing *Bohaiornis* and *Shenqiornis*; M. Wang et al., 2014). This result is in agreement with the recent discovery of other "bohaiornithid-like" taxa which shows only a subset of the features diagnostic of Bohaiornithidae (e.g., Chiappe et al., 2019): these results suggest that the "core" bohaiornithids are part of a more speciose "bohaiornithoid" radiation, including both small-bodied taxa (e.g., *Musivavis* n. gen.) and large-bodied taxa (e.g., *Gretcheniao*).

Conclusions

The unique combination of features of MHGU-3000 supports erection of a new genus and new species of Enantiornithes, *Musivavis amabilis* n. gen. n. sp., which enriches the diversity of the Jehol Biota birds. The mosaic of anatomical characters in *M. amabilis* n. gen. n. sp. and its smaller body size (presuming that the immature specimen would have reached only a marginally larger adult body size) differentiate it from the large-sized bohaiornithid enantiornithines, suggesting that this taxon occupied an ecological niche distinct from those of its closest relatives. Under all alternative scenarios tested, *Musivavis* n. gen. was part of a relatively rich clade with a wide range of adult body sizes and trophic adaptations. The reconstruction of enantiornithine relationships is affected by homoplasy and skeletal modularity. The homoplasy in the appendicular modules (in particular, the recurrent evolution of scansorial adaptations in the foot) might have a significant effect on the relative placements of Bohaiornithidae and Pengornithidae. The consistent reconstruction of the "bohaiornithid-grade," including *Musivavis* n. gen., under different downweighting settings supports the monophyly of this successful radiation of ecologically disparate enantiornithines.

Acknowledgments

We would like to thank M. Wang for preparing the specimen, K. Fang for preparing the histological sample, and S. Chen and P. Yin for conducting the CT scan and reconstructions. We also appreciate M. Pittman and three anonymous reviewers for their constructive comments on the early version of the manuscript. Many thanks go to D. Ksepka and J. Kastigar for their kind suggestions and attention. This work was supported by projects from the National Natural Science Foundation of China (41872018, 41672019), the China Geological Survey (DD20190602), the Scientific Grant Agency VEGA of the Ministry of the Education, Science, Research and Sport of the Slovak Republic (1/0075/22) and the Slovak Research and Development Agency (APVV-18-0251).

Data availability statement

Data available from the Dryad Digital Repository: https://doi.org/10.5061/dryad.5tb2rbp5k.

References

Alvarenga, H.M., and Bonaparte, J.F., 1992, A new flightless land bird from the Cretaceous of Patagonia, *in* Campbell, K.C., ed., Papers in Avian Paleontology Honoring Pierce Brodkorb. Los Angeles, Natural History Museum of Los Angeles County, v. 36, p. 51–64.

Bailleul, A.M., O'Connor, J.K., Li, Z., Wu, Q., Zhao, T., Martinez, M.M., Wang, M., and Zheng, X., 2020, Confirmation of ovarian follicles in an enantiornithine (Aves) from the Jehol biota using soft tissue analyses: Communications Biology, v. 3, 399. https://doi.org/10.1038/s42003-020-01131-9.

Baumel, J.J., King, A.S., Breazile, J.E., Evans, H.E., and Vanden Berge, J.C., 1993, Handbook of Avian Anatomy: Nomina Anatomica Avium, Second Edition: Cambridge, Massachusetts, Publications of the Nuttall Ornithological Club, no. 23, p. 1–779.

Cambra-Moo, O., Buscalioni, Á.D., Cubo, J., Castanet, J., Loth, M-M., de Margerie, E., and de Ricqlès, A., 2006, Histological observations of Enantiornithine bone (Saurischia, Aves) from the Lower Cretaceous of Las Hoyas (Spain): Comptes Rendus Palevol, v. 5, p. 685–691.

Cau, A., 2018, The assembly of the avian body plan: a 160 million year long process: Bollettino della Società Paleontologica Italiana, v. 57, p. 1–25.

Chiappe, L.M., 1995, The phylogenetic position of the Cretaceous birds of Argentina: Enantiornithes and *Patagopteryx deferrariisi*: Courier Forschungsinstitut Senckenberg, v. 181, p. 55–63.

Chiappe, L.M., 2002, Basal bird phylogeny: problems and solutions, *in* Chiappe, L.M., and Witmer, L.M., eds., Mesozoic Birds: Above the Heads of Dinosaurs: Berkeley, University of California Press, p. 448–472.

Chiappe, L.M, and Meng, Q., 2016, Birds of Stone: Chinese Fossils from the Age of Dinosaurs: Baltimore, Johns Hopkins University Press, 108 p.

Chiappe, L.M., and Walker, C.A., 2002, Skeletal morphology and systematics of the Cretaceous Euenantiornithes (Ornithothoraces: Enantiornithes), *in* Chiappe, L.M., and Witmer, L.M., eds., Mesozoic Birds: Above the Heads of Dinosaurs: Berkeley, University of California Press, p. 240–267.

Chiappe, L.M., Meng, Q., Serrano, F., Sigurdsen, T., Wang, M., Bell, A., and Liu, D., 2019, New *Bohaiornis*-like bird from the Early Cretaceous of China: enantiornithine interrelationships and flight performance: PeerJ, v. 7, e7846. https://doi.org/10.7717/peerj.7846.

Chinsamy, A., and Elzanowski, A., 2001, Evolution of growth pattern in birds: Nature, v. 412, p. 402–403.

Chinsamy, A., Chiappe, L.M., and Dodson, P., 1995, Mesozoic avian bone microstructure: physiological implications: Paleobiology, v. 21, p. 561–574.

Dalsätt, J., Ericson, G.P., and Zhou, Z., 2014, A New Enantiornithes (Aves) from the Early Cretaceous of China: Acta Geologica Sinica (English Edition), v. 88, p. 1034–1040.

de Ricqlès, A., Meunier, F.J., Castanet, J., and Francillon-Vieillot, H., 1991, Comparative microstructure of bone, *in* Hall, B.K, ed., Bone, Matrix and Bone Specific Products: Boca Raton, Florida, CRC Press, v. 3, p. 1–78.

Elzanowski, A., 1974, Preliminary note on the palaeonathous birds from the Upper Cretaceous of Mongolia. Results of the Polish-Mongolian paleontological expeditions—part V: Palaeontologia Polonica, v. 30, p. 103–109.

Gauthier, J.A., 1986, Saurischian monophyly and the origin of birds, *in* Padian K., ed., The Origin of Birds and the Evolution of Flight: San Francisco, California Academy of Science, p. 1–55.

Goloboff, P.A., Farris, J.S., and Nixon, K.C., 2008, TNT, a free program for phylogenetic analysis: Cladistics, v. 24, p. 774–786.

Hou, L., 1997, Mesozoic Birds in China: Taiwan, Phoenix Valley Bird Garden Press, 84 p. [in Chinese]

Hou, L., Martin, L.D., Zhou, Z., and Feduccia, A., 1999, *Archaeopteryx* to opposite birds—missing link from the Mesozoic of China: Vertebrata Palasiatica, v. 37, p. 88–95.

Hu, D., Li, L., Hou, L., and Xu, X., 2011, A new enantiornithine bird from the Lower Cretaceous of western Liaoning, China: Journal of Vertebrate Paleontology, v. 31, p. 154–161.

Hu, H., and O'Connor, J.K., 2017, First species of Enantiornithes from Sihedang elucidates skeletal development in Early Cretaceous enantiornithines: Journal of Systematic Palaeontology, v. 15, p. 909–926.

Hu, H., O'Connor, J.K., and Zhou, Z., 2015, A new species of Pengornithidae (Aves: Enantiornithes) from the Lower Cretaceous of China suggests a specialized scansorial habitat previously unknown in Early Birds: PLoS ONE, v. 10(6), e0126791. https://doi.org/10.1371/journal.pone.0126791.

Hu, H., O'Connor, J.K., Wang, M., Wroe, S., and McDonald, P.G., 2020, New anatomical information on the bohaiornithid *Longusunguis* and the presence of a plesiomorphic diapsid skull in Enantiornithes: Journal of Systematic Palaeontology, v. 18, p. 1481–1495.

Knoll, F., Chiappe, L.M., Sanchez, S., Garwood, R.J., Nicholas, P.E., Wogelius, R.A., Sellers, W.I., Manning, P.l., Ortega, F., Serrano, F.J., Marugán-Lobón, J., Cuesta, E., Escaso, F., and Sanz, J.L., 2018, A diminutive perinate European Enantiornithes reveals an asynchronous ossification pattern in early birds: Nature Communications, v. 9, 937. https://doi.org/10.1038/s41467-018-03295-9.

O'Connor, J.K., and Chiappe, L.M., 2011, A revision of enantiornithine (Aves: Ornithothoraces) skull morphology: Journal of Systematic Palaeontology, v. 9, p. 135–157.

O'Connor, J.K., and Dyke, G.J., 2010, A reassessment of *Sinornis santensis* and *Cathayornis yandica* (Aves: Enantiornithes), *in* Boles, W.E., and Worthy, T.H., eds., Proceedings of the VII International Meeting of the Society of Avian Paleontology and Evolution: Records of the Australian Museum, v. 62, p. 7–20.

O'Connor, J.K., Wang, X., Chiappe, L.M., Gao, C., Meng, Q., Cheng, X., and Liu, J., 2009, Phylogenetic support for a specialized clade of Cretaceous enantiornithine birds with information from a new species: Journal of Vertebrate Paleontology, v. 29, p. 188–204.

O'Connor, J.K., Chiappe, L.M., Gao, C., and Zhao, B., 2011, Anatomy of the Early Cretaceous Enantiornithine bird *Rapaxavis pani*: Acta Palaeontologica Polonica, v. 56, p. 463–475.

O'Connor, J.K., Zhang, Y., Chiappe, L.M., Meng, Q., Li, Q. and Liu, D., 2013, A new enantiornithine from the Yixian Formation with the first recognized avian enamel specialization: Journal of Vertebrate Paleontology, v. 33, p. 1–12.

O'Connor, J.K., Wang, X., Zheng, X., Hu, H., Zhang, X., and Zhou, Z., 2016, An enantiornithine with a fan-shaped tail, and the evolution of the rectricial complex in early birds: Current Biology, v. 26, p. 114–119.

O'Connor, J.K., Erickson, G.M., Norell, M., Bailleul, A.M., Hu, H., and Zhou, Z., 2018, Medullary bone in an Early Cretaceous enantiornithine bird and discussion regarding its identification in fossils: Nature Communications, v. 9, 5169. https://doi.org/10.1038/s41467-018-07621-z.

O'Connor, J.K., Zheng, X., Pan, Y., Wang, X., Wang, Y., Zhang, X., and Zhou, Z., 2020, New information on the plumage of *Protopteryx* (Aves: Enantiornithes) from a new specimen: Cretaceous Research, v. 116, 104577. https://doi.org/10.1016/j.cretres.2020.104577.

Sanz, J.L., and Buscalioni, A., 1992, A new bird from the Early Cretaceous of Las Hoyas, Spain, and the early radiation of birds: Paleontology, v. 35, p. 829–845.

Schweitzer, M.H., Jackson, F.D., Chiappe, L.M., Schmidt, J.G., Calvo, J.O., and Rubilar, D.E., 2002, Late Cretaceous avian eggs with embryos from Argentina: Journal of Vertebrate Paleontology, v. 22, p. 191–195.

Walker, C.A., 1981, New subclass of birds from the Cretaceous of South America: Nature, v. 292, p. 51–53.

Wang, M., and Liu, D., 2016, Taxonomical reappraisal of Cathayornithidae (Aves: Enantiornithes): Journal of Systematic Palaeontology, v. 14, p. 29–47.

Wang, W., and O'Connor, J.K., 2017, Morphological coevolution of the pygostyle and tail feathers in Early Cretaceous birds: Vertebrata PalAsiatica, v. 55, p. 289–314.

Wang, M., and Zhou, Z., 2019, A new enantiornithine (Aves: Ornithothoraces) with completely fused premaxillae from the Early Cretaceous of China: Journal of Systematic Palaeontology, v. 17, p. 1299–1312.

Wang, M., and Zhou, Z., 2020, Anatomy of a new specimen of *Piscivorenantiornis inusitatus* (Aves: Enantiornithes) from the Lower Cretaceous Jehol Biota: Journal of Vertebrate Paleontology, v. 40, 3. https://doi.org/10.1080/02724634.2020.1783278.

Wang, M., Zhou, Z., O'Connor, J.K., and Zelenkov, N.V., 2014, A new diverse enantiornithine family (Bohaiornithidae fam. nov.) from the Lower Cretaceous of China with information from two new species: Vertebrata PalAsiatica, v. 52, p. 31–76.

Wang, M., Liu, D., O'Connor, J.K., Zhou, Z., and You, H., 2015, Second species of enantiornithine bird from the Lower Cretaceous Changma Basin, northwestern China with implications for the taxonomic diversity of the Changma avifauna: Cretaceous Research, v. 55, p. 56–65.

Wang, M., Hu, H., and Li, Z., 2016, A new small enantiornithine bird from the Jehol Biota, with implications for early evolution of avian skull morphology: Journal of Systematic Palaeontology, v. 14, p. 481–497.

Wang, M., O'Connor, J.K., Pan, Y., and Zhou, Z., 2017, A bizarre Early Cretaceous enantiornithine bird with unique crural feathers and an ornithuromorph plough-shaped pygostyle: Nature Communications, v. 8, 14141. https://doi.org/10.1038/ncomms14141.

Wang, M., Li, Z., Liu, Q., and Zhou, Z., 2020, Two new Early Cretaceous ornithuromorph birds provide insights into the taxonomy and divergence of Yanornithidae (Aves: Ornithothoraces): Journal of Systematic Palaeontology, v. 18, p. 1805–1827.

Wang, M., Stidham, T.A., Li, Z., Xu, X., and Zhou, Z., 2021, Cretaceous bird with dinosaur skull sheds light on avian cranial evolution: Nature Communications, v. 12, 3890. https://doi.org/10.1038/s41467-021-24147-z.

Wang, X.-L, O'Connor, J.K., Zheng, X., Wang, M., Hu, H., and Zhou, Z., 2014, Insights into the evolution of rachis dominated tail feathers from a new basal enantiornithine (Aves: Ornithothoraces): Biological Journal of the Linnean Society, v. 113, p. 805–819.

Wang, X.-R, O'Connor, J.K., Zhao, B., Chiappe, L.M., Gao, C., and Cheng, X., 2010, New species of *Enantiornithes* (Aves: Ornithothoraces) from the Qiaotou Formation in northern Hebei, China: Acta Geologica Sinica (English Edition), v. 84, p. 247–256.

Wang, X.-R., Shen, C., Liu, S., Gao, C., Cheng, X., and Zhang, F., 2015, New material of *Longipteryx* (Aves: Enantiornithes) from the Lower Cretaceous Yixian Formation of China with the first recognized avian tooth crenulations: Zootaxa, v. 3941, p. 565–578.

Wang, X.-R, Huang, J., Kundrát, M., Cau, A., Liu, X., Wang, Y., Ju, S., 2020, A new jeholornithiform exhibits the earliest appearance of the fused sternum and pelvis in the evolution of avialan dinosaurs: Journal of Asian Earth Sciences, v. 199, p. 1–18.

Wang, Y., Wang, M., O'Connor, J.K., Wang, X.-L, Zheng, X., and Zhang, X., 2016, A new Jehol enantiornithine bird with three-dimensional preservation and ovarian follicles: Journal of Vertebrate Paleontology, v. 36. e1054496. https://doi.org/10.1080/02724634.2015.1054496.

Xu, G., Yang, Y., and Deng, S., 1999, First discovery of Mesozoic bird fossils in Hebei province and its significance: Regional Geology of China, v. 18, p. 444–448. [in Chinese with English abstract]

Xu, X., Zhou, Z., Wang, Y., and Wang, M., 2020, Study on the Jehol Biota: recent advances and future prospects: Science China (Earth Sciences), v. 63, p. 757–773.

Zhang, F., and Zhou, Z., 2000, A primitive enantiornithine bird and the origin of feathers: Science, v. 290, p. 1955–1959.

Zhang, F., Zhou, Z., Hou, L., and Gu, G., 2001, Early diversification of birds: evidence from a new opposite bird: Chinese Science Bulletin, v. 46, p. 945–950.

Zhang, Z., Chiappe, L.M., Han, G., and Chinsamy, A., 2013, A large bird from the Early Cretaceous of China: new information on the skull of enantiornithines: Journal of Vertebrate Paleontology, v. 33, p. 1176–1189.

Zheng, X., Martin, L.D., Zhou, Z., Burnham, D.A., Zhang, F., and Miao, D., 2011, Fossil evidence of avian crops from the Early Cretaceous of China: Proceedings of the National Academy of Sciences of the United States of America, v. 108, p. 15904–15907.

Zheng, X., O'Connor, J.K., Wang, X., Zhang, X., and Wang, Y., 2014, New information on Hongshanornithidae (Aves:Ornithuromorpha) from a new subadult specimen: Vertebrata PalAsiatica, v. 52, p. 217–232.

Zhou, S., Zhou, Z., and O'Connor, J.K., 2013, Anatomy of the basal ornithuromorph bird *Archaeorhynchus spathula* from the Early Cretaceous of Liaoning, China: Journal of Vertebrate Paleontology, v. 33, p. 141–152.

Zhou, Z., 1995, Discovery of a new enantiornithine bird from the Early Cretaceous of Liaoning, China: Vertebrata PalAsiatica, v. 33, p. 99–113.

Zhou, Z., 2002, A new and primitive enantiornithine bird from the Early Cretaceous of China: Journal of Vertebrate Paleontology, v. 22, p. 49–57.

Zhou, Z., 2014, The Jehol Biota, an Early Cretaceous terrestrial Lagerstätte: new discoveries and implications: National Science Review, v. 1, p. 543–559.

Zhou, Z., and Zhang, F., 2006, A beaked basal ornithurine bird (Aves, Ornithurae) from the Lower Cretaceous of China: Zoologica Scripta, v. 35, p. 363–373.

Zhou, Z., Jin, F., and Zhang, J., 1992, A preliminary study on the early Mesozoic bird fossils in Liaoning Province: Science Bulletin, v. 37, p. 435–437. [in Chinese with English abstract]

Zhou, Z., Chiappe, L.M., and Zhang, F., 2005, Anatomy of the Early Cretaceous bird *Eoenantiornis buhleri* (Aves: Enantiornithes) from China: Canadian Journal of Earth Sciences, v. 42, p. 1331–1338.

Accepted: 3 February 2022